Chemical Science

EDGE ARTICLE

View Article Online
View Journal | View Issue

CrossMark click for updates

Cite this: *Chem. Sci.*, 2015, **6**, 654

A macrocycle-assisted nanoparticlization process for bulk Ag_2S†‡

Xin He,[a] Yuechao Wang,[b] Cai-Yan Gao,[a] Hong Jiang[b] and Liang Zhao*[a]

Received 25th June 2014
Accepted 11th September 2014

DOI: 10.1039/c4sc01884b

www.rsc.org/chemicalscience

We report herein a new nanoparticlization process for the bulk-to-nano transformation of Ag_2S by incorporating both top-down and bottom-up approaches. Bulk Ag_2S was dissolved in solution with the assistance of a macrocyclic ligand, hexamethylazacalix[6]pyridine (**Py[6]**), to produce polynuclear silver sulfide cluster aggregates. All Ag–S cluster aggregates obtained in three crystalline complexes were protected by **Py[6]** macrocycles. Removing the protective **Py[6]** macrocycles by protonation led to the generation of unconventional Ag–S nanoparticles with a large energy gap. Theoretical calculations by a hybrid DFT method demonstrated that the silver sulfide clusters with high Ag/S ratio exhibited more localized HOMO–LUMO orbitals, which consequently enlarged their band gap energies. These experimental and theoretical studies broaden our understanding of the fabrication of nanomaterials by virtue of the advantages of both bottom-up and top-down methods and meanwhile provide a viable means of adjusting the band gap of binary nanomaterials independent of their size.

Introduction

Silver sulfide, a well-known type of direct and narrow band gap semiconductor,[1] has attracted considerable attention due to its good stability, low toxicity[2] and extensive potential applications in photovoltaic cells, photoconductors,[3] infrared detectors[4] and near-infrared imaging.[5] Besides a band gap of 0.9–1.1 eV for bulk α-Ag_2S,[6] diminishing the size of Ag_2S to the nanometer scale provides an efficient way to finely tune the band gap of this material based on the quantum confinement effect, thus resulting in many intriguing size-specific optical and optoelectronic properties.[7] In this regard, different synthetic methods[6] *e.g.* the microemulsion approach[8] and the hot injection method[9] have been comprehensively explored during the past two decades with the aim of achieving uniformly sized Ag_2S nanocrystals. However, the use of exotic ligand- or surfactant-stabilized silver and sulfide ions or their precursors and the requirement for elevated temperature and high pressure in most cases made these synthetic protocols arduous. Obviously, if bulk Ag_2S solid could be directly transformed into its nano-sized prototype, this would be a concise and ideal synthetic strategy. However, to the best of our knowledge, no reported method for the synthesis of silver chalcogenide nanomaterials involves such a direct transformation.

Recently, the synthesis of silver chalcogenide nanocluster compounds in crystalline form has been reported in the literature.[10,11] During the reaction between various silver thiolates (SR) and silylated sulfide sources in the presence of coordinative phosphane ligands, nanometer-sized Ag/S/SR silver clusters can be generated at room temperature, but amorphous Ag_2S is obtained on increasing the reaction temperature. Such biased reaction pathways suggest a possible intermediate role of silver sulfide clusters in the synthesis of silver sulfide nano-objects. Inspired by this understanding, we envision that successful transformation of bulk Ag_2S to silver sulfide nanomaterials could be initiated with the synthesis of polynuclear silver sulfide clusters directly from bulk Ag_2S. A combination of top-down (from bulk Ag_2S to silver sulfide clusters) and bottom-up (from silver sulfide clusters to nanomaterials) approaches may facilitate the bulk-to-nano transformation of Ag_2S. However, bulk Ag_2S is known for its very poor solubility ($K_{sp} = 8 \times 10^{-51}$ at 25 °C), which makes it a formidable challenge to dissolve bulk Ag_2S solid and complete the bulk-to-nano transformation by means of cluster intermediates. Very recently, we found that a new class of macrocycles, azacalix[*n*]pyridines (**Py[*n*]**), exhibited a positive allosteric effect upon binding with metal ions,[12] which significantly enhanced their affinity to a multimetallic aggregate and led to the formation of silver acetylide clusters by using slightly soluble polymeric $[RC{\equiv}CAg]_n$ as starting materials.[13]

[a]*The Key Laboratory of Bioorganic Phosphorus Chemistry & Chemical Biology (Ministry of Education), Department of Chemistry, Tsinghua University, Beijing 100084, China. E-mail: zhaolchem@mail.tsinghua.edu.cn*

[b]*Beijing National Laboratory for Molecular Sciences, State Key Laboratory of Rare Earth Materials Chemistry and Applications, Institute of Theoretical and Computational Chemistry, College of Chemistry and Molecular Engineering, Peking University, Beijing 100871, China*

† This work is dedicated to Professor Thomas C. W. Mak in celebration of his 78th birthday.

‡ Electronic supplementary information (ESI) available: Synthetic procedures and crystal structure determination details. Analytical data, spectra, and images. X-ray crystallographic data for **1–4** in CIF format. CCDC 1006732, 1006826, 1006827 and 1006830. For ESI and crystallographic data in CIF or other electronic format see DOI: 10.1039/c4sc01884b

We have thus conceived a synthetic strategy to implement the bulk-to-nano transformation of silver sulfide, as illustrated in Scheme 1. A particular polypyridine macrocyclic ligand **Py[*n*]** will be used to initially facilitate the formation of macrocycle-protected silver sulfide clusters based on its positive allosteric effect. Upon the interruption of coordination bonds between polypyridine ligands and silver atoms *via* protonation, the encapsulated silver sulfide clusters may mutually coalesce to finally produce silver sulfide nanoparticles, which can be stabilized by additional surfactants.

Results and discussion

Considering the high efficiency of **Py[6]** (composed of six 1,3-pyridine rings bridged by six N–CH_3 moieties)[14] in our previous synthesis of a silver ethynediide cluster-encapsulated supramolecular capsule,[13b] we firstly attempted to utilize this macrocyclic ligand to dissolve Ag_2S solid. When Ag_2S solid was added to a methanol solution of $AgCF_3SO_3$ (0.2 M), no obvious color change of the solution was observed. However, addition of **Py[6]** into the Ag_2S–$AgCF_3SO_3$ mixture led to the appearance of a yellow color very quickly and a gradual decrease in the amount of Ag_2S solid, suggesting the dissolution of Ag_2S. It should be noted that silver triflate is essential for dissolving Ag_2S solid, since mixing only Ag_2S with **Py[6]** does not cause any color change. We next carried out ^{1}H-NMR analysis of the reaction mixture of Ag_2S–$AgCF_3SO_3$–**Py[6]**. In the ^{1}H-NMR spectrum, there were three triplet peaks at 8.05 (Ha), 7.87 (Hb) and 7.60 (Hc) ppm corresponding to the pyridyl γ-protons of **Py[6]** (Fig. 1a). A typical downfield shift of these peaks relative to neat **Py[6]** (7.46 ppm for pyridyl γ-protons)[14] suggested the occurrence of coordination between **Py[6]** and silver ions. Furthermore, diffusion ordered spectroscopy (DOSY) exhibited two diffusion bands (Fig. 1b), implying the existence of two dominant assembled species in the reaction mixture. As shown in Fig. 1b, the species corresponding to the signal Hb (denoted as **A**) has a larger diffusion coefficient than the other species (denoted as **B**) accounting for the signals Ha and Hc. The diameter ratio of **A** to **B** in the classical spherical model was deduced as 0.80 based on their respective diffusion coefficients and the Stokes–Einstein equation, which agrees quite well with the ratio (0.78) of the measured distances between the two most separated points of the functional units in the crystal structures of **1** and **2** *vide infra*.

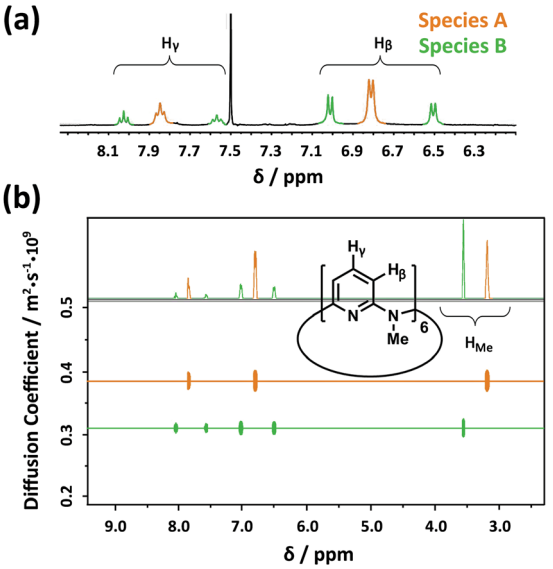

Fig. 1 (a) Partial ^{1}H NMR spectrum (400 MHz, $CDCl_3$: methanol-d_4 (v/v) = 1 : 1, 25.0 °C) and (b) DOSY spectrum of the reaction mixture of $AgCF_3SO_3$, Ag_2S and **Py[6]**.

The NMR titration experiment of **Py[6]** with silver triflate clarified that the species **A** was actually derived from the assembly of silver triflate and **Py[6]**, due to identical proton NMR spectra (see Fig. S1 in the ESI‡). Single crystals of the species **A** (denoted as crystalline complex **1**) for X-ray crystallographic analysis were deposited from the CH_3OH–CH_2Cl_2 mixed solution of **Py[6]** and $AgCF_3SO_3$. As shown in Fig. 2a, the ratio of silver triflate to **Py[6]** in complex **1** was determined as 3 : 1, giving the formula of **1** as $\{Ag_3(\mathbf{Py[6]})(CF_3SO_3)_3(H_2O)_{0.5}\}$. The central silver atom Ag1 in **1** adopted a linear coordination geometry to bind with the two opposite pyridines of the **Py[6]**, thus causing the formation of a cage-like structure. This unimolecular folding fashion is similar to our previously reported scenarios for two larger macrocycles **Py[8]** and **Py[9]**.[12]

The structural analysis of species **B** was complicated. High-resolution mass spectroscopy (HR-MS) of the Ag_2S–$AgCF_3SO_3$–**Py[6]** yellow reaction mixture revealed two isotopically well-resolved peaks at m/z = 1258.9341 and 554.9862 corresponding to the $[(CF_3SO_3)_2Ag_3(\mathbf{Py[6]})]^+$ and $[(CF_3SO_3)Ag_3(\mathbf{Py[6]})]^{2+}$ species (Fig. S2‡), confirming the existence of species **A**. In addition, several peaks corresponding to the species composed of a **Py[6]** macrocycle and a polynuclear silver sulfide cluster plus some silver triflate groups were found by HR-MS (Fig. S2‡). For example, a strong peak at m/z = 1762.5754 can be ascribed to the species $[Ag_6S(\mathbf{Py[6]})(CF_3SO_3)_3]^+$ and the peak at m/z = 934.7313 is isotopically in good agreement with the species $[Ag_7S(\mathbf{Py[6]})(CF_3SO_3)_3]^{2+}$. We then conducted a

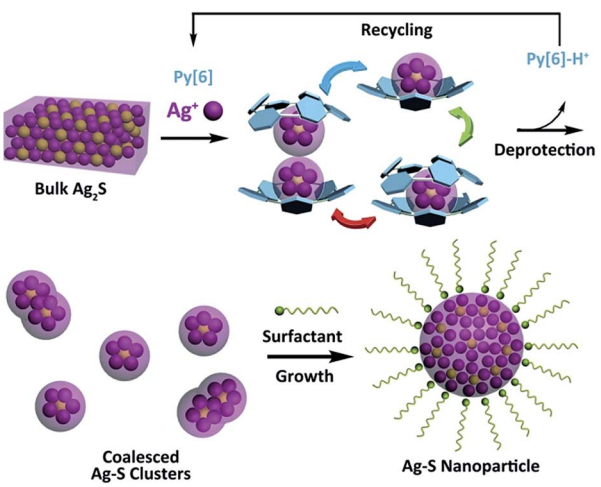

Scheme 1 Macrocycle-assisted bulk-to-nano transformation of Ag_2S.

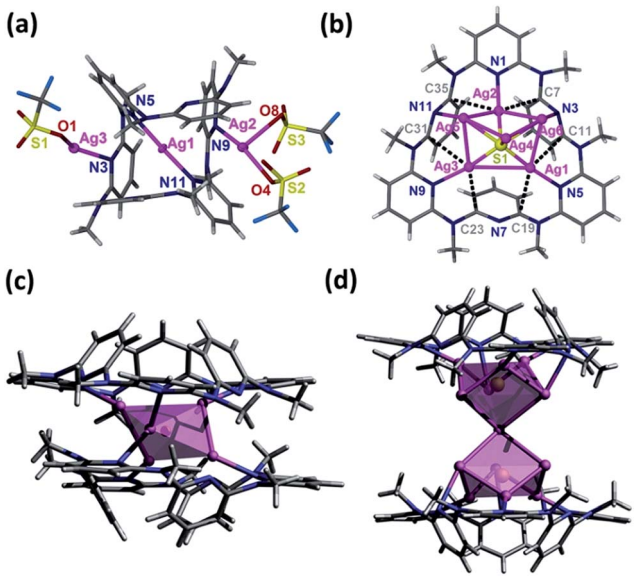

Fig. 2 (a) Crystal structure of complex $\{Ag_3(\mathbf{Py[6]})(CF_3SO_3)_3(H_2O)_{0.5}\}$ (**1**). Selected bond distances (Å): Ag1–N5 2.154(3); Ag1–N11 2.168(3); Ag2–N9 2.281(4); Ag3–N3 2.284(3). (b) Partial crystal structure of $[Ag_5S(\mathbf{Py[6]})](CF_3SO_3)_3\cdot CH_3OH$ (**2**). Ag5 and Ag6 each have an occupancy ratio of 0.5. The three triflate groups on the top side of the $[Ag_5–S]$ cluster are omitted for clarity. Silver–aromatic π interactions are shown by dashed lines. Ag–C distances (Å): Ag1–C11 2.987; Ag1–C19 2.948; Ag2–C7 2.731; Ag2–C35 2.957; Ag3–C23 2.836; Ag3–C31 3.090. (c) Side view of complex $[Ag_5S(\mathbf{Py[6]})_2](CF_3SO_3)_3$ (**3**) with the central silver sulfide cluster represented by a polyhedron. (d) Crystal structure of $[Ag_{12}S_2(\mathbf{Py[6]})_2](CF_3SO_3)_8\cdot H_2O\cdot CH_3OH$ (**4**). Two silver atoms each have an occupancy ratio of 0.5. Triflate groups and solvent molecules are omitted for clarity. Color scheme for atoms: Ag, purple; C, gray; H, white; N, blue; S, yellow; F, cyan.

crystallization process by adding diethyl ether to the reaction mixture, and a crystalline compound with the formula of $[Ag_5S(\mathbf{Py[6]})](CF_3SO_3)_3\cdot(CH_3OH)$ (**2**) was finally obtained. The crystal structure of **2** (Fig. 2b) comprises a central sulfur anion that is enclosed by six silver atoms, two of which (Ag5 and Ag6) each have an occupancy ratio of 0.5. This silver sulfide cluster is properly described as a $[Ag_5–S]$ aggregate, which is coordinated by a **Py[6]** macrocycle on one side and is further bonded to three triflate anions on another side. Argentophilic interactions[15] and silver–aromatic π interactions both play a significant role in the stabilization of such a $[Ag_5–S]$ cluster situated inside a **Py[6]** macrocycle. Interestingly, a similar crystallization process but with a longer crystallization time than that for complex **2** resulted in a new crystalline complex **3**, which has a formula of $[Ag_5S(\mathbf{Py[6]})_2](CF_3SO_3)_3$ based on its crystal structure analysis. As shown in Fig. 2c, complex **3** also comprises a $[Ag_5–S]$ aggregate with C_2-axis symmetry, which is protected by two face-to-face **Py[6]** ligands to give a cluster-embedded supramolecular capsule. To the best of our knowledge, this is the first example of a discrete silver sulfide cluster with an inner penta-coordinated sulfide.[16] This $[Ag_5–S]$ structural motif is also consistent with the basic structural unit of bulk Ag_2S.[17] But in contrast, the Ag–S bond lengths in **3** (2.369(3)–2.432(4) Å) are ~0.2 Å shorter than the values for bulk Ag_2S[17] and other silver sulfide clusters.[11,16,18] Another crystalline complex $[Ag_{12}S_2(\mathbf{Py[6]})_2](CF_3SO_3)_8\cdot H_2O\cdot CH_3OH$ (**4**) was serendipitously acquired upon reducing the amount of **Py[6]** employed in the above synthetic procedure for complex **2**. As shown in Fig. 2d, the dumbbell-shaped $[Ag_{12}S_2]$ silver sulfide cluster aggregate in **4** can be described as two single sulfide-centered cage-like silver clusters fused by sharing a middle silver atom. In addition, the upper and lower sides of this dumbbell-shaped silver cluster are enclosed by two **Py[6]** macrocycles similarly to **3**. The total seven silver atoms in the asymmetric unit of **4** share a refined site occupancy of six, since silver atom Ag6 is located at a position of special symmetry while Ag7 is disordered, and both have a refined site occupancy ratio of less than one (see ESI for details‡). Despite the structural difference of the silver sulfide clusters between complexes **2–4** both in nuclearity number and cluster configuration, the **Py[6]** macrocycles in **2–4** all adopt a similar quasi-C_{3v} bowl-shaped conformation. Moreover, we substantiated that most silver sulfide cluster species in the reaction mixture of Ag_2S, $AgCF_3SO_3$ and **Py[6]** were stabilized by one or two **Py[6]** macrocyclic ligands. In addition, based on the HR-MS and ^{1}H-NMR data and the DOSY result that reflected a size ratio (0.80) comparable to the value of 0.78 in the crystal structures of **1** and **2**, we hypothesized that complex **2**, which is composed of a **Py[6]** macrocycle and a polynuclear silver sulfide cluster, is probably the second dominant species (species **B**) in the reaction mixture of Ag_2S, $AgCF_3SO_3$ and **Py[6]**.

The successful isolation of discrete (in **2** and **3**) and joint (in **4**) silver sulfide clusters by varying the amount of the protective **Py[6]** proves the viability of synthesizing Ag–S binary nanoparticles through the coalescence and fusion of silver sulfide clusters. In view of the fact that **Py[6]** can be easily protonated by a strong acid due to the good Lewis basicity of pyridine, we added CF_3COOH into the filtrate of the reaction mixture of Ag_2S, $AgCF_3SO_3$ and **Py[6]** to interrupt the coordination interactions between the central silver sulfide cluster and the surrounding **Py[6]** macrocycles. The dismantlement of **Py[6]** led to a clear yellow solution. This solution sample retained its yellow color for an hour, but further standing resulted in a black precipitate. The formation and stepwise growth of metal sulfide nanoparticles was affirmed by transmission electron microscopy (TEM) photographs prepared at different intervals (Fig. 3a–b). We subsequently employed oleic amine[9] as a surfactant to stabilize the obtained nanoparticles. The resulting yellow solution can retain its solution homogeneity for several days. TEM images of this solution sample (denoted as **D-NP**) substantiated the formation of metal nanoparticles with an average diameter of 4 ± 0.4 nm (Fig. 3c). Fourier transform IR spectroscopy analysis of a solid sample of **D-NP** prepared by centrifugation clearly showed the absence of **Py[6]** and the presence of oleic amine molecules in **D-NP** (Fig. S3‡). This observation verified our above assumption that **Py[6]**-protected silver sulfide clusters could indeed undergo a deprotection process to act as nuclei and activated monomers for the fabrication of silver sulfide nanoparticles. Notably, we found that the acidified **Py[6]** ligands can be recycled after neutralization and

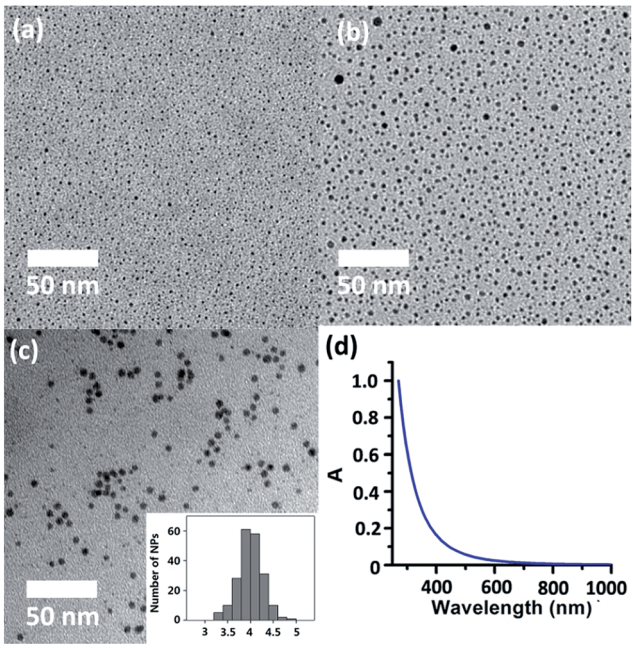

Fig. 3 TEM images of deprotected silver sulfide clusters following the addition of CF_3COOH (a) after 30 s and (b) after 2 min. (c) TEM images of sample **D-NP**. (inset) Size-distribution histogram of silver sulfide nanoparticles in **D-NP**. (d) UV-vis spectrum of **D-NP** in cyclohexane at 298 K.

extraction and then employed for subsequent bulk-to-nano transformation of silver sulfide.

On the other hand, high-resolution TEM (HR-TEM) of **D-NP** showed very ambiguous lattice fringes, in contrast to the clear pattern in previously reported Ag_2S nanoclusters,[19] suggesting a poorly crystalline form of **D-NP**. The low crystallinity of **D-NP** was further substantiated by selected area electron diffraction (SAED) (Fig. S4‡), which exhibited two weak diffraction rings that could be indexed to the (−103) and (232) facets of monoclinic Ag_2S (JCPDS card 14-0072). Energy dispersive X-ray spectroscopy (EDX) measurements of **D-NP** indicated the presence of elements Ag and S and further gave a Ag/S atomic ratio of 3.5 (Fig. S5‡). We also conducted XPS analysis of **D-NP**. As reflected in the XPS experiment (Fig. S6‡), we confirmed the +1 oxidation state of the silver atoms in **D-NP** based on their Ag $3d^{5/2}$ and Ag $3d^{3/2}$ binding energy peaks at 374.5 and 368.5 eV, respectively. In addition, the Ag/S molar ratio was determined to be 3.7 based on the XPS data, which is comparable to the energy dispersive X-ray spectroscopy (EDX) result of 3.5. This Ag/S elemental ratio in **D-NP** is larger than the values of around 2.0 in bulk Ag_2S[17] and previously reported silver sulfide nanoclusters.[1,3,19] We hypothesized that such a high Ag/S ratio in **D-NP** may arise from the coalescence and fusion of the silver-rich Ag–S clusters in **2–4** by forming inter-cluster interactions (*e.g.*, argentophilicity) and sharing silver atoms similarly to the above-mentioned scenarios in **4**. In addition, the absorption spectrum of the cyclohexane solution of **D-NP** (Fig. 3d) exhibited a monotonic decrease in the whole recorded range, which is similar to the spectra of a number of reported silver sulfide nanocluster samples.[3c,5b] The band gap energy could be fitted by using the Bardeen or Tauc equations (Fig. S7‡). The direct transition of **D-NP** was thus deduced to be 4.0 eV, largely blue-shifted relative to the band gap of bulk α-Ag_2S.[6] It is noteworthy that modifying the composition ratio of different constituents in nanomaterials in order to perform band gap adjustment has been frequently applied in ternary and quaternary alloyed semiconductor nanomaterials, but rarely in binary systems.[20] The method reported herein represents a viable means to tune the band gap of binary nanomaterials independent of their size.

In order to clarify the relationship between the energy gap and the Ag/S ratio in silver sulfide clusters, we carried out a theoretical HOMO–LUMO gap calculation of silver sulfide clusters with different Ag/S ratios *via* a hybrid density functional theory (DFT) method (see calculation details in the ESI‡). It is highly challenging to construct a structural model and optimize the structure of a 4 nm Ag–S cluster. We thus carried out the calculation on four small Ag–S clusters (Ag_8S_4, $Ag_{10}S_5$, $Ag_{11}S_3(OH)_5$ and $Ag_{12}S_3(OH)_6$) with different Ag : S ratios (Fig. 4). The initial structures of the four clusters were built up according to the reported structural motifs of α-Ag_2S[17] and the crystal structures of silver sulfide clusters.[10,11] For the sake of simplifying the structural optimization and energy gap computation, hydroxyl groups were used in substitution of the coordinated peripheral $CF_3SO_3^-$ and $CF_3CO_2^-$ anions in the calculation for silver sulfide clusters with an Ag/S ratio larger than two. As reflected in the calculated results (Table S1‡), the two clusters Ag_8S_4 and $Ag_{10}S_5$ with an Ag/S ratio of two have HOMO–LUMO energy gaps of 2.45 and 1.86 eV, respectively. In contrast, the other two size-comparable clusters $Ag_{11}S_3(OH)_5$ and $Ag_{12}S_3(OH)_6$ with an Ag/S ratio larger than 2 have corresponding energy gaps of 3.11 and 3.09 eV. These calculated results agree well with the trend in our above experiment. Compared with the two clusters Ag_8S_4 and $Ag_{10}S_5$, $Ag_{11}S_3(OH)_5$ and $Ag_{12}S_3(OH)_6$ with a higher Ag : S elemental ratio exhibited more localized HOMO–LUMO orbitals (Fig. 4 and S8‡). The less dispersed orbitals in these two Ag–S clusters ultimately led to the band gap enlargement.

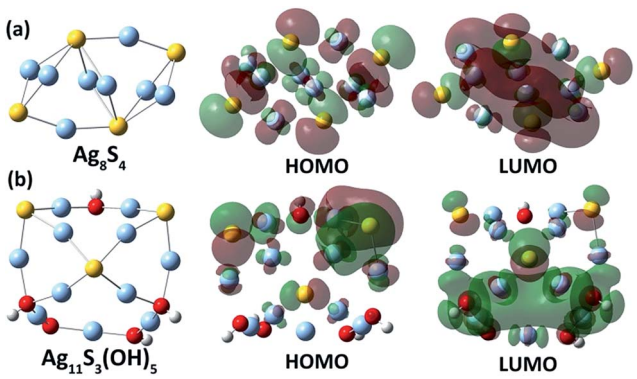

Fig. 4 Optimized structures of two Ag–S clusters with different Ag/S elemental ratios, (a) Ag_8S_4 and (b) $Ag_{11}S_3(OH)_5$, and their HOMO and LUMO orbitals.

Conclusions

In summary, we have demonstrated a viable means of synthesizing silver sulfide nanomaterials directly from the bulk form with the assistance of coordinative macrocyclic ligands. This method could be successfully applied in the fabrication of other binary silver nanomaterials such as silver halides, acetylides *etc.*, based on our recent investigation. Considering that the size of macrocyclic ligands can dominate the nuclearity number of the obtained metal cluster aggregates, this approach can also be employed to achieve nanomaterials with different properties dependent on different nucleation centers. Following this study, we foresee the synthesis of numerous new nanomaterials with novel properties based on a synthetic revisiting inspired by the combination of bottom-up and top-down methods reported herein.

Acknowledgements

Financial support by the MOST (973 program, 2013CB834501 and 2011CB932501) and NNSFC (91127006, 21132005, 21121004) is gratefully acknowledged. This work is also supported by MOE (NCET-12-0296), Tsinghua University Initiative Scientific Research Program (2011Z02155) and Beijing Higher Education Young Elite Teacher Project (YETP0130). We are grateful to Profs. Mei-Xiang Wang and De-Xian Wang for their helpful discussion.

Notes and references

1 (*a*) K. Akamatsu, S. Takei, M. Mizuhata, A. Kajinami, S. Deki, S. Takeoka, M. Fujii, S. Hayashi and K. Yamamoto, *Thin Solid Films*, 2000, **359**, 55; (*b*) W. P. Lim, Z. Zhang, H. Y. Low and W. S. Chin, *Angew. Chem., Int. Ed.*, 2004, **43**, 5685.

2 P. Hirsch, *Environ. Toxicol. Chem.*, 1998, **17**, 601.

3 (*a*) K. Terabe, T. Hasegawa, T. Nakayama and M. Aono, *Nature*, 2005, **433**, 47; (*b*) F. Gao, Q. Y. Lu and D. Y. Zhao, *Nano Lett.*, 2003, **3**, 85; (*c*) V. M. Huxter, T. Mirkovic, P. S. Nair and G. D. Scholes, *Adv. Mater.*, 2008, **20**, 2439; (*d*) W. J. Lou, X. B. Wang, M. Chen, W. M. Liu and J. C. Hao, *Nanotechnology*, 2008, **19**, 225607; (*e*) J. H. Xiang, H. Q. Cao, Q. Z. Wu, S. C. Zhang, X. R. Zhang and A. A. R. Watt, *J. Phys. Chem. C*, 2008, **112**, 3580; (*f*) Y. Lei, H. Jia, W. He, Y. Zhang, L. Mi, H. Hou, G. Zhu and Z. Zheng, *J. Am. Chem. Soc.*, 2012, **134**, 17392; (*g*) B. Liu, D. Wang, Y. Zhang, H. Fan, Y. Lin, T. Jiang and T. Xie, *Dalton Trans.*, 2013, **42**, 2232; (*h*) P.-J. Wu, J.-W. Yu, H.-J. Chao and J.-Y. Chang, *Chem. Mater.*, 2014, **26**, 3485.

4 G. Hodes, J. Manassen and D. Cahen, *Nature*, 1976, **261**, 403.

5 (*a*) Y. Du, B. Xu, T. Fu, M. Cai, F. Li, Y. Zhang and Q. Wang, *J. Am. Chem. Soc.*, 2010, **132**, 1470; (*b*) M. Yarema, S. Pichler, M. Sytnyk, R. Seyrkammer, R. T. Lechner, G. Fritz-Popovski, D. Jarzab, K. Szendrei, R. Resel, O. Korovyanko, M. A. Loi, O. Paris, G. Hesser and W. Heiss, *ACS Nano*, 2011, **5**, 3758; (*c*) G. Hong, J. T. Robinson, Y. Zhang, S. Diao, A. L. Antaris, Q. Wang and H. Dai, *Angew. Chem., Int. Ed.*, 2012, **51**, 9818.

6 S. V. Kershaw, A. S. Susha and A. L. Rogach, *Chem. Soc. Rev.*, 2013, **42**, 3033.

7 (*a*) A. Tubtimtae, K. Wu, H. Tung, M. Lee and G. Wang, *Electrochem. Commun.*, 2010, **12**, 1158; (*b*) R. Wang, R. Tangirala, S. Raoux, J. Jordan-Sweet and D. Milliron, *Adv. Mater.*, 2012, **24**, 99; (*c*) E. Kong, Y. Chang, H. Park and H. Jang, *Small*, 2014, **10**, 1300.

8 (*a*) V. Buschmann, G. Van Tendeloo, P. Monnoyer and J. B. Nagy, *Langmuir*, 1998, **14**, 1528; (*b*) X. Jiang, Y. Xie, J. Lu, L. Zhu, W. He and Y. Qian, *J. Mater. Chem.*, 2001, **11**, 584.

9 D. Wang, T. Xie, Q. Peng and Y. Li, *J. Am. Chem. Soc.*, 2008, **130**, 4016.

10 (*a*) J. F. Corrigan, O. Fuhr and D. Fenske, *Adv. Mater.*, 2009, **21**, 1867; (*b*) O. Fuhr, S. Dehnen and D. Fenske, *Chem. Soc. Rev.*, 2013, **42**, 1871.

11 G. Li, Z. Lei and Q.-M. Wang, *J. Am. Chem. Soc.*, 2010, **132**, 17678.

12 X. He, X.-B. Xu, X. Wang and L. Zhao, *Chem. Commun.*, 2013, **49**, 7153.

13 (*a*) C.-Y. Gao, L. Zhao and M.-X. Wang, *J. Am. Chem. Soc.*, 2011, **133**, 8448; (*b*) C.-Y. Gao, L. Zhao and M.-X. Wang, *J. Am. Chem. Soc.*, 2012, **134**, 824; (*c*) C.-Y. Gao, X. He, L. Zhao and M.-X. Wang, *Chem. Commun.*, 2012, **48**, 8368; (*d*) X. He, C.-Y. Gao, M.-X. Wang and L. Zhao, *Chem. Commun.*, 2012, **48**, 10877.

14 E.-X. Zhang, D.-X. Wang, Q.-Y. Zheng and M.-X. Wang, *Org. Lett.*, 2008, **10**, 2565.

15 (*a*) M. Jansen, *Angew. Chem., Int. Ed. Engl.*, 1987, **26**, 1098; (*b*) P. Pyykkö, *Chem. Rev.*, 1997, **97**, 597.

16 Discrete μ_4-S silver cluster: V. W.-W. Yam, K. K.-W. Lo, C.-R. Wang and K.-K. Cheung, *Inorg. Chem.*, 1996, **35**, 5116.

17 D. Santamaría-Pérez, M. Marqués, R. Chuliá-Jordán, J. M. Menendez, O. Gomis, J. Ruiz-Fuertes, J. A. Sans, D. Errandonea and J. M. Recio, *Inorg. Chem.*, 2012, **51**, 5289.

18 R. Ahlrichs, A. Eichhöfer, D. Fenske, O. Hampe, M. M. Kappes, P. Nava and J. Olkowska-Oetzel, *Angew. Chem., Int. Ed.*, 2004, **43**, 3823.

19 (*a*) A. Sahu, L. Qi, M. S. Kang, D. Deng and D. J. Norris, *J. Am. Chem. Soc.*, 2011, **133**, 6509; (*b*) R. Rica and A. H. Velders, *J. Am. Chem. Soc.*, 2011, **133**, 2875; (*c*) Y. Zhang, Y. Liu, C. Li, X. Chen and Q. Wang, *J. Phys. Chem. C*, 2014, **118**, 4918.

20 (*a*) J. M. Luther and J. M. Pietryga, *ACS Nano*, 2013, **7**, 1845; (*b*) S. J. Oh, N. E. Berry, J.-H. Choi, E. A. Gaulding, T. Paik, S.-H. Hong, C. B. Murray and C. R. Kagan, *ACS Nano*, 2013, **7**, 2413.